Multiple-Screen Diffraction Measurement at 10–18 GHz

Glaucio Lopes Ramos, Pekka Kyösti, Veikko Hovinen, and Matti Latva-aho

***Abstract*—This letter presents analysis of diffraction over multiple shadowing screens at frequency range of 10–18 GHz. Up to ten pieces of thin metal sheets with dimensions of 130 × 100 cm at variable spacing were used as diffraction screens. The aim of this study is to investigate the total shadowing effect of multiple knife-edge diffractions at frequencies above the legacy cellular systems. The results show the necessity to adjust the Walfisch–Bertoni path loss model for the higher frequencies in the future fifth-generation systems.**

***Index Terms*—Centimeter-wave (cmWave) and millimeter-wave (mmWave) measurements, multiple-screen diffraction loss, Walfisch–Bertoni settled-field equation.**

I. Introduction

CENTIMETER-WAVE (cmWave) and millimeter-wave (mmWave) range, above the traditional cellular frequency bands, has been promising for the fifth-generation (5G) telecommunication systems. Several measurements and research activities have recently been conducted to investigate the frequency range to be utilized by the coming 5G systems around 2020 and beyond [1]–[6].

The demand for higher transmission rates, when compared to existing systems operating below 3 GHz, has motivated the use of millimeter-wave spectrum, as a large range of spectrum is available within the 3–30-GHz super high-frequency and 30–300-GHz extremely high-frequency spectrum. In this way, radio channel characterization becomes essential within the mentioned spectra in order to design and foresee the operation of the new 5G systems.

A semideterministic channel model for evaluation of 5G systems was developed and proposed by the METIS Project in [7]. The introduced map-based model addresses the variety of requirements set to a 5G channel model. One important aspect of the model is the concept of random objects. It is known that the blockage is a prominent propagation effect on higher frequencies and that the existing 4G models are not sufficiently covering this effect [7], [8]. In the map-based model, the objects, representing smaller obstacles such as lamp posts, humans, and cars, cause blockage of propagation paths. In [7], for the shadowing effect, the objects are approximated as conductive rectangular screens. The attenuation due to an object is modeled with the knife-edge diffraction across four edges of the screen. This offers a relatively simple method to calculate the shadowing effect as a function of frequency and geometry.

In the case of dense population of objects, as for example with many humans in an open-air festival, the multiple knife-edge diffraction overestimates the attenuation. Therefore, a special amendment for multiple-screen shadowing was introduced in [7]. There the knife-edge diffraction is taken only for the dominant object and the model is complemented by an additional diffraction loss due to multiple screens, approximated by the Walfisch–Bertoni model [9], [10]. However, the original Walfisch–Bertoni model has been derived from a set of measurement conducted in the 1980s and earlier at below 1-GHz frequencies and with tens-of-kilometers link distances. Thus, it may not be fully suitable with higher frequencies, much shorter link distances, and shorter interobject distances. The original motivation for our current work is to evaluate, by measurements, whether the original Walfisch–Bertoni model is suitable for complementing the 5G blockage model of [7] and to find an updated parameterization for it, if found necessary.

Only a few diffraction measurements are available at the 10–18-GHz frequency band [6]. To the knowledge of the authors, no measurements results for the excess diffraction path loss in a multiple screen shadowing environment exist in the literature.

The letter is organized as follows. Section II presents the Walfisch–Bertoni diffraction excess loss (EL) equation. Section III describes the measurement setup and environment. The data analysis process and measurement results are presented in Section IV. The conclusions are discussed in Section V.

II. Walfisch–Bertoni Diffraction Approximation

The Walfisch–Bertoni model accounts for a multiple-diffraction environment. In this model, a numerical evaluation of the Kirchhoff–Huygens integral has been performed, and a power, law formula has been obtained for the field settled with sufficient large number of obstacles (buildings) [10]. The ratio of the settled-field and the incident-field amplitudes, which can

This work was supported in part by the CNPq 446648/2014-0 and CAPES/PROCAD 068419/2014-01, and in part by the Finnish Funding Agency for Technology and Innovation (Tekes), Huawei Technologies, Nokia, and Keysight Technolo-gies Finland Oy within the framework of 5G to 10G Project. *(Corresponding author: Glaucio Lopes Ramos.)*

G. L. Ramos is with the Antennas and Propagation Research Group, Federal University of São João del-Rei, São João del-Rei 36307-352, Brazil (e-mail: glopesr@gmail.com).

P. Kyösti is with the Centre for Wireless Communications, University of Oulu, Oulu 90014, Finland, and also with Keysight Technologies Finland Oy, Oulu 90590, Finland (e-mail: pekka.kyosti@keysight.com).

V. Hovinen and M. Latva-aho are with the Centre for Wireless Communications, University of Oulu, Oulu 90590, Finland (e-mail: veikko.hovinen@oulu.fi; matti.latva-aho@oulu.fi).

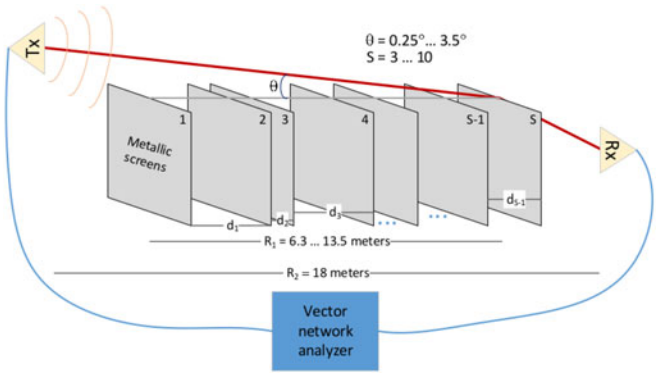

Fig. 1. Block diagram of the radio channel measurement setup.

be considered as the excess diffraction loss, is defined as

$$A_{\text{settled}} \approx 0.1\left(\frac{\theta}{0.03}\sqrt{\frac{d_{av}}{\lambda}}\right)^{0.9} = 2.35\left(\theta\sqrt{\frac{d_{av}}{\lambda}}\right)^{0.9} \quad (1)$$

where θ is the elevation angle of the base station antenna from the top of the final building in radians, d_{av} is the average distance between the buildings, and λ is the free-space wavelength [10]. This equation accounts for multiple diffraction in contrast to the single-edged diffraction from the first building and at first can be applied when $0.03 \leq t \leq 0.4$, where $t = \theta\sqrt{\frac{d_{\text{av}}}{\lambda}}$, and also requires a large number of buildings, particularly when θ is small.

In this letter, the performance of this settled-field approximation will be evaluated for some environment conditions that probably will occur in 5G future systems, particularly for many closely spaced objects (screens) between the transmitter and receiver and for small values of θ. Equation (1) will be generalized to the following form:

$$A_{\text{settled}} = a\left(\theta\sqrt{\frac{d_{av}}{\lambda}}\right)^{b} \quad (2)$$

where the original parameter values are $a = 2.35$ and $b = 0.9$.

III. Measurement Setup

The overall measurement configuration is illustrated in Fig. 1. The intention was to perform a number of static network analyzer measurements varying both the incidence angle θ and the interscreen spacing. The measurements were performed inside an auditorium at the University of Oulu.

The screens, up to ten, were metallic plates with dimensions of $130 \times 100 \times 0.05$ cm^3. To analyze different diffraction scenarios, the screens' average distance was changed, resulting in six different screens configurations, with different average distance between screens, as described in Table I. The screens were placed typically in nonuniform spacing. Only the screen position closest to the RX antenna was fixed at the distance of 1.5 m from the antenna. The total two-dimensional distance from the transmitter (TX) to the receiver (RX) was 18 m.

The antenna configuration was single-input–single-output (SISO), with a RX antenna height of 1.147 m and TX antenna height of 1.37, 1.445, 1.59, 1.735, 1.88, 2.02, 2.165, and 2.31 m. The measured bandwidth was 8 GHz (10–18 GHz), wide enough to enable time-gating of multipath components resulting from interactions with the other environment, such as wall and floor reflections. The purpose is to investigate only the paths diffracted over the screens. Additional absorbers were placed on both sides of the first and the last screen to suppress propagation across the vertical screen edges. A photograph of the measured environment can be seen in Fig. 2.

TABLE I
Multiple-Screen Configuration

Configuration	Number of screens	Average distance d_{av}
1	10	1.28
2	10	1.50
3	7	2.25
4	6	2.30
5	5	3.38
6	3	6.75

A Keysight N5227A 4-port PNA network analyzer was utilized to record the scattering parameters (S_{21} parameters) in the frequency domain. The transmit power was 10 dBm, the number of points was settled to 3201, and the resolution bandwidth (IFBW) 10 kHz. The TX antenna was an SH-2000 dual-ridged Satimo horn (2–32 GHz) with return loss <-10 dB over the 10–18-GHz frequency band. The RX antenna was an SH-4000 dual-ridged Satimo horn (4–40 GHz) with return loss < -10 dB over the 10–18-GHz frequency band. Radiation patterns of antennas were measured with Satimo Starlab. Antenna gains in the main direction are in the range of 7.3 and 10.7 dBi (RX) and 10.3 and 13.1 dBi (TX) on the measurement band. The antenna gain variation across the small range of utilized departure/arrival angles is negligible, thus a single gain value per antenna per frequency band can be used. In the measurement, both antennas were oriented to have vertical main polarization.

IV. Data Analysis and Results

At first, the EL due to multiple-screen diffraction is analyzed from the measurements. Then, the function of (2) is fitted to the extracted data to find the function parameters a, b.

A. Extracting Excess Diffraction Loss

The inverse discrete Fourier transform (IDFT) was applied to obtain impulse responses of the channel. A sliding Kaiser window with parameter $\beta = 5$ was applied in IDFT to weight the data to different center frequencies and to prevent the frequency leakage. The measurement settings using a bandwidth of 8 GHz provide a delay resolution of 0.125 ns, a path resolution of 3.75 cm, and a maximum detectable path length of 120 m. Once the delay domain of the measured channel was obtained, the diffracted path was selected assuming the first detected multipath component is the diffracted one. The path length d of this path from the TX antenna to the RX antenna was also checked for each configuration.

In the multiple-screen shadowing model [7], [9], [10], the first dominating shadowing screen closest to RX is approximated using the knife-edge diffraction model [11], and the additional diffraction loss due to multiple screens is estimated using the

Fig. 2. Panorama view of the measurement environment. (Screens were aligned in a straight row formation, despite the optical impression of the photograph.)

previous defined Walfisch–Bertoni equation. Therefore, when processing the measured data for each screen configuration, the first peak power level is obtained. The measured path gain $G(d, \theta, f, \Theta)$, where Θ denotes the screen configuration, is then obtained. The antenna gains g_{rx} and g_{tx}, the free-space path loss L_{fsl}, as well as the knife-edge diffraction loss L_{ked} for the screen closest to RX are compensated for. The remaining effect is assumed to be the EL due to multiple screens, calculated as follows:

$$A_{\text{meas}}(d, \theta, f, \Theta) = \sqrt{\frac{G(d, \theta, f, \Theta) L_{\text{fsl}}(d, f) L_{\text{ked}}(\theta, f)}{g_{\text{tx}}(f) g_{\text{rx}}(f)}} \quad (3)$$

where all gains and losses are in linear power units.

B. Determining Walfisch–Bertoni Function Parameters

Once the excess diffraction loss was obtained separately for each screen configuration, each incidence angle, and each frequency under analysis, a search for the coefficients of the Walfisch–Bertoni EL, (2), was also performed. The results of all measured configurations were processed altogether, and a best fit for the coefficients a and b was obtained for each frequency under analysis. The fit was done using the MATLAB Curve Fitting Toolbox using a custom equation in the format of (1), in decibels units. The best a and b values were found using goodness-of-fit statistics.

The fitted curve for 10-GHz measurements data can be seen in Fig. 3, and the results of all bands are summarized in Table II. At 10 GHz, for small values of θ and d_{av} in the range of 1.28 and 6.75 m, we can observe a similar result for the b coefficient and an offset of 3.4 dB because of the a coefficient difference, when compared to the original Walfisch–Bertoni equation.

From Table II, we get the mean values $a = 1.419$ and $b = 0.9762$ for the parameters averaged over all the analyzed frequency bands.

Based on the extracted parameters of Table II and their stable behavior across considered frequency bands, we propose to update the Walfisch–Bertoni parameters in (1) using the mean obtained values $a = 1.419$ and $b = 0.9762$. The updated function based on measurement results is an approximation of observations from (3) and confirms the need to calibrate the Walfish–Bertoni diffraction EL for the mmWave frequency range. Even

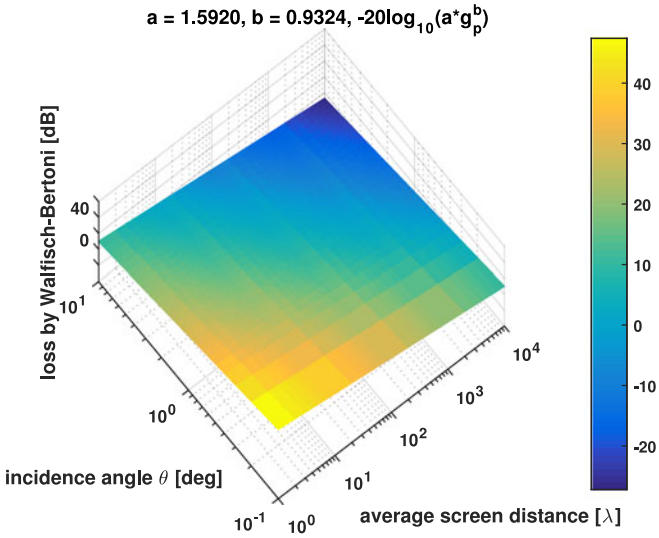

Fig. 3. Fit curve: 10-GHz measurements.

TABLE II
FITTED PARAMETERS—(2)

Frequency	a	b
10 GHz	1.592	0.9324
11 GHz	1.535	0.9445
12 GHz	1.458	0.9522
13 GHz	1.374	0.9654
14 GHz	1.439	0.9767
15 GHz	1.341	0.9878
16 GHz	1.318	0.9986
17 GHz	1.365	1.0090
18 GHz	1.350	1.0190
Mean value	**1.419**	**0.9762**

while the b parameter is closer to the original, a significant offset of approximately 4.4 dB was found with the a parameter extracted from the measurements.

This difference can be explained by a set of reasons. The environment is highly different: Obstacles are uniform 1.3-m-high metallic screens instead of heterogeneous outdoor urban

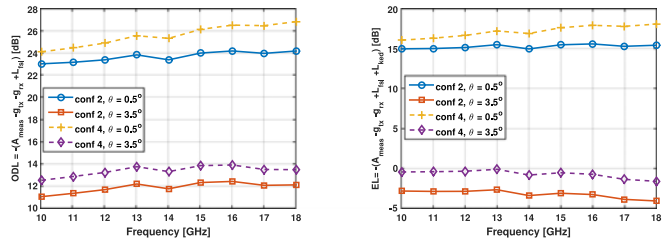

(a) (b)

Fig. 4. Results for the (a) ODL and (b) EL.

environment with mostly concrete-made high-rise buildings. There was typically never any knife edge diffraction in the original Walfisch–Bertoni measurements. Rather, there the condition was wedge diffraction from building rooftops and roof structures. Also, the frequency in the current work is more than one decade higher compared to the original Walfisch–Bertoni measurements. We propose to substitute the original Bertoni parameters only for the special purpose of the METIS map-based model [7], but not the original model for urban microcellular environments at UHF bands or higher bands.

Using the mean values of a and b, the EL can be extrapolated to higher interspace screen distance (in wavelengths). The t parameter must be in the $0.03 \leq t \leq 0.997$ range in order for the EL to be positive and also to be in the range of this measurement campaign. The updated function can be utilized for modeling of multiple-screen diffraction for the cases described in [7, Sec 6.2, step 7]. We expect that the applicable frequency range for the model can be well extended also beyond the original measurement band of 10–18 GHz.

C. Frequency Dependency of Diffraction Loss

Frequency dependence of the overall measured diffraction loss (ODL) and its comparison to the EL is illustrated in Fig. 4. For the ODL case, the antenna gains and the theoretical free-space loss are compensated from the measured gain of the diffracted path (over screens). For the EL case, the knife-edge diffraction loss from the first screen (closest to Rx) is also compensated.

With $\theta = 0.5^\circ$ in the configuration 2, there is line-of-sight (LOS) blockage for the first six screens, resulting in an approximate ODL of 23.7 dB and an approximate EL of 15.3 dB (an 8.4-dB difference from the mean ODL) and for configuration 4, there is LOS blockage for the first four screens, resulting in an approximate ODL of 25.6 dB and an approximate EL of 17.2 dB (an 8.4-dB difference from the mean ODL. The screen density, six or ten screens, has only modest impact to the loss.

With $\theta = 3.5^\circ$, there is LOS blockage only by the first screen. The mean ODL is approximately 11.8 dB and the mean EL is approximately -3.3 dB (a 15.1-dB difference from the mean ODL) for the configuration 2, and the mean ODL is 13.3 dB and the mean EL is -0.8 dB (a 14.1-dB difference from the mean ODL) for the configuration 4. We can observe negative ELs (gain) for this case, and this can be explained by the contribution of the other screens (diffraction to the lit zone), which on average generates a diffraction gain when considering the contributions altogether. For this case, the screen density, six or ten screens, has only modest impact to the loss.

V. Conclusion

In this letter, diffraction measurements in a multiple-screen environment were performed at a frequency range of 10–18 GHz. These results could be useful to be considered in RF prediction for the new 5G communications systems, especially for the blockage effect.

A radio channel measurement setup using a vector network analyzer (VNA), directive TX and RX antennas, and up to ten metallic screens was configured in an open space, and the excess diffraction loss was extracted from the measurements. The main objective was to verify and update the Walfisch–Bertoni excess diffraction loss coefficients, which originally have the values of $a = 2.35$ and $b = 0.9$, when applied to the cmWave and mmWave frequency bands predictions and with substantially smaller link distances and interobstacle distances as the original model.

Finally, the measurements showed that it is necessary to make a small calibration in the Walfisch–Bertoni excess diffraction loss, when applying it at the cmWave and mmWave frequency bands, in a multiple-object shadowing environment for blockage modeling with obstacles of relatively small sizes in meters. The analysis gave new coefficients, with values of $a = 1.419$ (which differs substantially from the original equation) and $b = 0.976$.

Future investigations could be considered for higher frequency bands, e.g., 25–60 GHz, with wider range of link distances and interscreen distances, with different screen sizes, and with both vertically and horizontally polarized measurement antennas.

References

[1] S. Salous *et al.*, "Millimeter-wave propagation: Characterization and modeling toward fifth-generation systems. [wireless corner]," *IEEE Antennas Propag. Mag.*, vol. 58, no. 6, pp. 115–127, Dec. 2016.

[2] J. Medbo *et al.*, "Radio propagation modeling for 5G mobile and wireless communications," *IEEE Commun. Mag.*, vol. 54, no. 6, pp. 144–151, Jun. 2016.

[3] K. Haneda, N. Omaki, T. Imai, L. Raschkowski, M. Peter, and A. Roivainen, "Frequency-agile pathloss models for urban street canyons," *IEEE Trans. Antennas Propag.*, vol. 64, no. 5, pp. 1941–1951, May 2016.

[4] P. B. Papazian, C. Gentile, K. A. Remley, J. Senic, and N. Golmie, "A radio channel sounder for mobile millimeter-wave communications: System implementation and measurement assessment," *IEEE Trans. Microw. Theory Techn.*, vol. 64, no. 9, pp. 2924–2932, Sep. 2016.

[5] A. Roivainen *et al.*, "Validation of deterministic radio channel model by 10 GHz microcell measurements," in *Proc. 22th Eur. Wireless Conf. Eur. Wireless 2016*, 2016, pp. 1–6.

[6] N. Tervo *et al.*, "Diffraction measurements around a building corner at 10 GHz," in *Proc. 1st Int. Conf. 5G Ubiquitous Connectivity*, 2014, pp. 1187–191.

[7] L. Rachowski, P. Kyösti, K. Kusume, and T. Jämsä, "METIS channel models, deliverable 1.4 v.1.3," METIS Project, Tech. Rep. ICT-317669, 2015.

[8] 3rd Generation Partnership Project, "Channel model for frequency spectrum above 6 GHz," 3rd Generation Partnership Project, Tech. Rep. TR 38.900, Rel 14, V2.0.0, Jun. 2016.

[9] H. L. Bertoni, *Radio Propagation for Modern Wireless Systems*, 1st ed. Englewood Cliffs, NJ, USA: Prentice-Hall, 2000.

[10] J. Walfisch and H. L. Bertoni, "A theoretical model of UHF propagation in urban environments," *IEEE Trans. Antennas Propag.*, vol. 36, no. 12, pp. 1788–1796, Dec. 1988.

[11] S. R. Saunders and A. Aragón-Zavala, *Antennas and Propagation for Wireless Communications Systems*, 2nd ed. New York, NY, USA: Wiley, 2007.